Low-frequency characterization of quantum tunneling in flux qubits

Ya.S. Greenberg,[1,*] A. Izmalkov,[1] M. Grajcar,[2,†] E. Il'ichev,[1,‡] W. Krech,[2]
H.-G. Meyer,[1] M.H.S. Amin,[3] and Alec Maassen van den Brink[3]

[1] *Institute for Physical High Technology, P.O. Box 100239, D-07702 Jena, Germany*
[2] *Department of Solid State Physics, FSU Jena, Germany*
[3] *D-Wave Systems Inc., 320-1985 W. Broadway, Vancouver, B.C., V6J 4Y3, Canada*

(Dated: February 1, 2008)

We propose to investigate flux qubits by the impedance measurement technique (IMT), currently used to determine the current–phase relation in Josephson junctions. We analyze in detail the case of a high-quality tank circuit coupled to a persistent-current qubit, to which IMT was successfully applied in the classical regime. It is shown that low-frequency IMT can give considerable information about the level anticrossing, in particular the value of the tunneling amplitude. An interesting difference exists between applying the ac bias directly to the tank and indirectly via the qubit. In the latter case, a convenient way to find the degeneracy point *in situ* is described. Our design only involves existing technology, and its noise tolerance is quantitatively estimated to be realistic.

PACS numbers: 74.50.+r, 84.37.+q, 03.67.-a

I. INTRODUCTION

Josephson-junction flux qubits are known to be candidates for solid-state quantum computing circuits.[1] This qubit variety has good tolerance to external noise, especially to dangerous background-charge fluctuations.[2] A flux qubit is a superconducting loop, the two lowest-energy states of which differ in the direction of circulating persistent current. For many flux qubits, these two states become degenerate when the external flux Φ_x threading the loop equals $\Phi_0/2$ ($\Phi_0 = h/2e$ is the flux quantum), and quantum tunneling between them becomes possible. Moving Φ_x away from $\Phi_0/2$ lifts the degeneracy and applies a bias between the two states. When the biasing energy exceeds the tunneling amplitude Δ the tunneling stops, but the relative phase between the two states will still evolve in time. This, together with coherent tunneling, provides single-bit quantum gate operations. To have a universal set of gates, necessary for quantum computing, one needs to be able to couple two qubits. The methods of coupling two flux qubits and performing gate operations are beyond the present scope. Instead, we propose a method to characterize the quantum behavior of a flux qubit by coupling it to a tank circuit. The discussion will be quite general and can be applied to different types of flux qubit such as rf-SQUID,[3] three-Josephson-junction (3JJ),[4,5] multi-terminal,[6] etc. We will use the example of the 3JJ qubit, where quantum superposition of the macroscopic current states has been observed.[5]

Due to the loop self-inductance, the total qubit flux Φ may differ from Φ_x, depending on the direction of the persistent current. Figure 1 shows the Φ–Φ_x curve for a typical flux qubit. The solid lines correspond to classical behavior. Near the degeneracy point, the diagram is hysteretic, a signature of the qubit's bistability. This has been observed for the 3JJ in Refs. 7,8. In the quantum regime, tunneling between the states at degeneracy may eliminate the hysteresis (dashed line in Fig. 1). This phenomenon will be discussed in detail below.

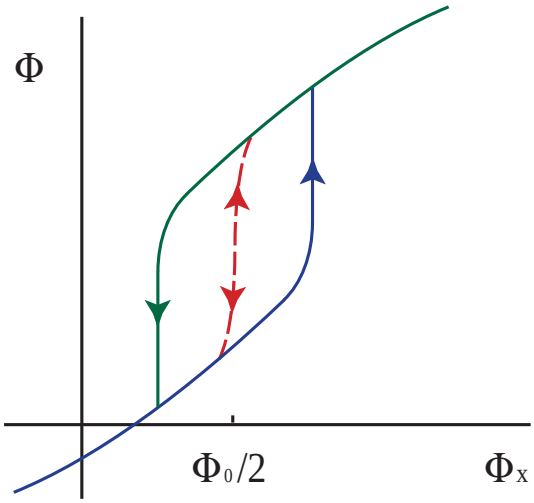

FIG. 1: Solid lines: hysteretic dependence of the total flux Φ on the external flux Φ_x in the classical regime. Dashed line: disappearance of the hysteresis by quantum tunneling.

In general, one can plot the classical (local) minimum energies of a flux qubit as in Fig. 2a. The left (right) branch then corresponds to (counter-)clockwise flow of the spontaneous current. The hysteresis is also evident from this diagram. In the quantum regime, there will be discrete local states in each of the qubit's bistable potential wells. From now on we denote the lowest-lying such states as Ψ^l and Ψ^r, corresponding to "left" and "right" directions of the persistent current respectively. At $\Phi_x = \Phi_0/2$, resonant tunneling will render the lowest eigenstates of the full Hamiltonian as superpositions $(\Psi^l \pm \Psi^r)/\sqrt{2}$. A small splitting equal to 2Δ will appear between their energies (Fig. 2b). Starting with the qubit in its ground state (lower band in Fig. 2b), adiabatically changing Φ_x will keep it in the ground state. This means that by passing through the degeneracy point, the qubit

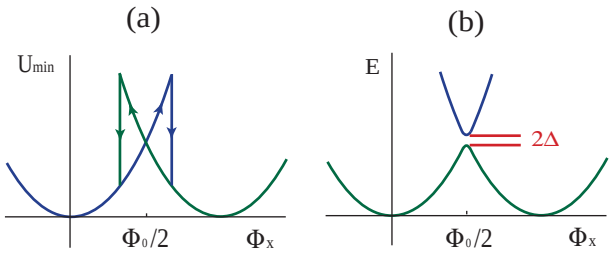

FIG. 2: (a) Minimum energies of a qubit as a function of external magnetic flux in the classical regime. (b) Quantum mechanical energy profile for the same qubit as in (a).

will continuously transform from $\Psi^{\rm l}$ to $\Psi^{\rm r}$. This pure quantum behavior is shown by the dashed line in Fig. 1. On the other hand, if $\Phi_{\rm x}$ changes rapidly, there is a considerable probability to excite the qubit and therefore continue on the same classical branch (left or right). This so-called Landau–Zener effect can be used to distinguish the classical from the quantum energy curves.

The curvature of the energy profile is related to the qubit's effective inductance and is therefore important for measurement. Figure 3 displays the second derivative of the curves in Fig. 2. In the classical regime (Fig. 3a), the hysteretic behavior is the same as for the energy. On the other hand, in the quantum regime the hysteresis is replaced by a sharp spike, due to the level anticrossing. The appearance of this spike can be ascribed to enhanced susceptibility of the system due to tunneling. Its size and width can provide information about Δ.

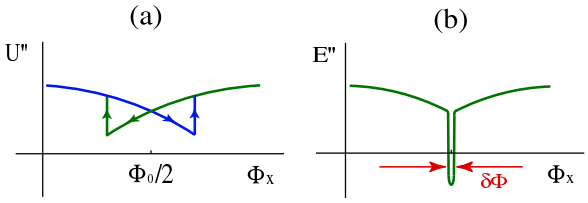

FIG. 3: (a) Second derivative of the qubit's classical minimum energy vs external magnetic flux. (b) Second derivative of the same qubit's ground-state energy in the quantum regime.

A simple experimental implementation is to inductively couple the qubit to an LC tank circuit with known inductance $L_{\rm T}$, capacitance $C_{\rm T}$, and quality Q through a mutual inductance M (Fig. 4). The resonant characteristics of the tank circuit (frequency, phase shift, etc.) will then be sensitive to the qubit inductance and therefore to its energy curvature. In particular, the spike in Fig. 3b appears as sharp dips in both phase shift and tank voltage as a function of $\Phi_{\rm x}$ (see Section III).

This method, known as *impedance measurement technique* (IMT), has been used for current–phase measurements of Josephson junctions. It originates from the pioneering work of Rifkin and Deaver,[9] and is analyzed in detail in Ref. 10. IMT has also successfully been applied

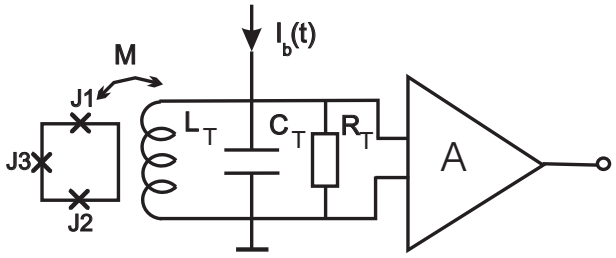

FIG. 4: Flux qubit coupled to a tank: direct biasing scheme.

to a 3JJ qubit in the classical regime,[8] and the hysteretic dependence of the ground-state energy on $\Phi_{\rm x}$ (cf. Fig. 2a) was observed as predicted in Ref. 4. The method has also been used for the investigation of quantum transitions in an rf-SQUID (Ref. 11 and references therein).

First of all, in Section II we calculate the two qubit energies in more detail than in Ref. 4. In Section III, we study the qubit's interaction with a high-quality resonant tank, showing that low-frequency IMT yields useful information about the qubit's quantum behavior. Finally, in Section IV, the effect of noise is considered.

II. QUANTUM DYNAMICS OF THE 3JJ QUBIT

The 3JJ qubit[4] consists of three Josephson junctions in a loop with very small inductance L, typically in the pH range. This insures effective decoupling from the environment. Two junctions have equal critical current $I_{\rm c}$ and (effective) capacitance C, while those of the third junction are slightly smaller: $\alpha I_{\rm c}$ and αC, with $0.5 < \alpha < 1$. If the Josephson energy $E_{\rm J} = I_{\rm c}\Phi_0/2\pi$ is much larger than the Coulomb energy $E_C = e^2/2C$, the Josephson phase is well defined. Near $\Phi_{\rm x} = \Phi_0/2$, this system has two low-lying quantum states.[4,12] The energy splitting between them in the presence of a small flux bias has been given in Ref. 5, but only for a particular choice of, e.g., α and $g \equiv E_{\rm J}/E_C$. In this section we derive the splitting with its explicit dependence on the qubit parameters. The energy levels are derived from the Hamiltonian [see Eq. (12) in Ref. 4]

$$H_0 = \frac{P_\varphi^2}{2M_\varphi} + \frac{P_\theta^2}{2M_\theta} + U(f_{\rm x},\varphi,\theta)\ , \qquad (1)$$

where $\varphi = (\varphi_1+\varphi_2)/2$, $\theta = (\varphi_1-\varphi_2)/2$ with $\varphi_{1,2}$ the phase differences across the two identical junctions, $P_\varphi = -i\hbar\partial_\varphi$, $P_\theta = -i\hbar\partial_\theta$, $M_\varphi = (\Phi_0/2\pi)^2 2C$, $M_\theta = (1+2\alpha)M_\varphi$, and

$$U(f_{\rm x},\varphi,\theta) = E_{\rm J}[\alpha - 2\cos\varphi\cos\theta + \alpha\cos(2\pi f_{\rm x}+2\theta)]\ . \quad (2)$$

In contrast to Ref. 4, we define the flux bias $f_{\rm x} = \Phi_{\rm x}/\Phi_0 - \frac{1}{2}$ as a small deviation from degeneracy.

Since the qubit is assumed to have small L and $I_{\rm c}$ (typically $L \approx 10$ pH, $I_{\rm c} \approx 100$ nA), the shielding factor

$LI_c/\Phi_0 \approx 0.001$. Hence, in (1) we have neglected the shielding current, considering Φ as an external flux.

At $f_x = 0$, the potential (2) has two minima at $\varphi = 0$, $\theta = \pm\theta_*$, with $\cos\theta_* = 1/2\alpha$ ($\theta_* > 0$). Tunneling lifts their degeneracy, leading to energy levels $E_\pm = \varepsilon_0 \pm \Delta$. To find the levels for $|f_x| \ll 1$ we expand Eq. (2) near its minima, retaining linear terms in f_x and quadratic terms in ϕ, θ. Define $\theta_*^{r/l}$ as the minima, shifted due to f_x:

$$\theta_*^{r/l} = \pm\theta_* + 2\pi f_x \frac{1-2\alpha^2}{4\alpha^2-1} \; ; \tag{3}$$

that is, the upper (lower) sign refers to the right (left) well. The potential energy then reads

$$\frac{U}{E_J} = -\frac{1}{2\alpha} \mp f_x \frac{\pi}{\alpha}\sqrt{4\alpha^2-1} + \frac{\varphi^2}{2\alpha}\left(1 \pm 2\pi f_x \frac{2\alpha^2-1}{\sqrt{4\alpha^2-1}}\right) + \left(\theta - \theta_*^{r/l}\right)^2 \left(2\alpha - \frac{1}{2\alpha} \pm f_x \frac{\pi}{\alpha}\frac{2\alpha^2+1}{\sqrt{4\alpha^2-1}}\right). \tag{4}$$

Near degeneracy, the eigensolutions of $H_0\Psi_\pm = E_\pm\Psi_\pm$ can be written as superpositions $\Psi_\pm = a_\pm\Psi^l + b_\pm\Psi^r$, yielding the well-known eigenenergies $E_\pm = (\varepsilon^l+\varepsilon^r)/2 \pm \sqrt{(\varepsilon^l-\varepsilon^r)^2/4 + \Delta^2}$, with $\varepsilon^{r/l} = \langle\Psi^{r/l}|H_0|\Psi^{r/l}\rangle$. The matrix element Δ cannot accurately be found in terms of $\Psi^{r/l}$. In what follows it is assumed constant,

$$\Delta = 2E_J\sqrt{\frac{2\alpha-1}{\alpha g}} \times \exp\left[\sqrt{\frac{g(2\alpha+1)}{\alpha}}\left(\arccos\frac{1}{2\alpha} - \sqrt{4\alpha^2-1}\right)\right], \tag{5}$$

neglecting its dependence on f_x.

To find the dependence of $E_\pm$ on f_x, we take $\Psi^{r/l}$ to be oscillator ground states in their respective wells:

$$\Psi^{r/l} = \frac{1}{\sqrt{\hbar\pi}}\left(M_\varphi\omega_\varphi^{r/l}M_\theta\omega_\theta^{r/l}\right)^{1/4} \times \exp\left(-\frac{M_\varphi\omega_\varphi^{r/l}}{2\hbar}\varphi^2 - \frac{M_\theta\omega_\theta^{r/l}}{2\hbar}\left(\theta-\theta_*^{r/l}\right)^2\right), \tag{6}$$

corresponding to

$$\varepsilon^{r/l} = E_J\left(-\frac{1}{2\alpha} \mp f_x\frac{\pi}{\alpha}\sqrt{4\alpha^2-1}\right) + \frac{\hbar\omega_\varphi^{r/l}}{2} + \frac{\hbar\omega_\theta^{r/l}}{2} \; , \tag{7}$$

where

$$\hbar\omega_\varphi^{r/l} = E_J\sqrt{\frac{4}{\alpha g}}\left(1 \pm \pi f_x\frac{2\alpha^2-1}{\sqrt{4\alpha^2-1}}\right), \tag{8}$$

$$\hbar\omega_\theta^{r/l} = E_J\sqrt{\frac{4(2\alpha-1)}{\alpha g}}\left(1 \pm \pi f_x\frac{2\alpha^2+1}{(4\alpha^2-1)^{3/2}}\right). \tag{9}$$

Combining the above, one finds the eigenenergies

$$E_\pm = \varepsilon_0 \pm \sqrt{E_J^2 f_x^2\lambda^2(\alpha) + \Delta^2} \; , \tag{10}$$

where

$$\varepsilon_0 = E_J\left(-\frac{1}{2\alpha} + \frac{1+\sqrt{2\alpha-1}}{\sqrt{\alpha g}}\right), \tag{11}$$

$$\frac{\alpha}{\pi}\lambda(\alpha) = \sqrt{\frac{\alpha}{g}}\left(\frac{2\alpha^2-1}{\sqrt{4\alpha^2-1}} + \frac{2\alpha^2+1}{\sqrt{2\alpha+1}(4\alpha^2-1)}\right) - \sqrt{4\alpha^2-1} \; . \tag{12}$$

The splitting given by Eq. (10) differs from that of Eq. (1) in Ref. 5 by a factor $\lambda(\alpha)$ which explicitly accounts for the dependence of $E_\pm$ on α and g.

For stationary states, the current in the qubit loop can be calculated either as the average of the current operator $\hat{I}_q = I_c\sin(\varphi+\theta)$ over the eigenfunctions, or as the derivative of the energy over the external flux:

$$I_q = \langle\Psi_\pm|\hat{I}_q|\Psi_\pm\rangle = \frac{\partial E_\pm}{\partial\Phi} = \pm I_c f_x\frac{\lambda^2(\alpha)}{\pi}\frac{E_J}{\hbar\omega_0} \; , \tag{13}$$

where $\hbar\omega_0 = E_+ - E_-$. In equilibrium at finite temperature T, Eq. (13) readily generalizes to

$$I_q = \langle\Psi_+|\hat{I}_q|\Psi_+\rangle\rho_{++}^{eq} + \langle\Psi_-|\hat{I}_q|\Psi_-\rangle\rho_{--}^{eq} = -I_c\frac{E_J f_x\lambda^2(\alpha)}{\pi\hbar\omega_0}\tanh\left(\frac{\hbar\omega_0}{2k_BT}\right) \tag{14}$$

with the density matrix elements $\rho_{++}^{eq} = e^{-E_+/k_BT}/Z$ and $\rho_{--}^{eq} = e^{-E_-/k_BT}/Z$, where $Z = e^{-E_+/k_BT} + e^{-E_-/k_BT}$.

III. QUBIT–TANK INTERACTION

We propose here to extract information about the quantum dynamics of a flux qubit with the aid of a classical linear high-quality tank circuit, coupled to the qubit via a mutual inductance M. The tank consists of a capacitor C_T, inductor L_T, and a resistor R_T which are connected in parallel and driven by a current source $I_b(t)$ (Fig. 4). The problem of coupling a quantum object to a dissipative classical one has no unique theoretical solution. However, if we assume that the classical object is much slower than the quantum one we may solve for the latter's motion, accounting for the coupling coordinates of the former as mere external parameters.[11] Here, the characteristic frequency Δ/h of the qubit is in the GHz range, while the resonances ω_T of our tank circuit lie below 100 MHz. There exist two different schemes of coupling a tank circuit to the qubit. First we consider direct biasing, where a current $I_b(t) = I_0\cos\omega t$ is fed directly into L_T (Fig. 4).

A. Direct biasing scheme

The voltage across the tank circuit evolves as

$$\ddot{V} + \frac{\omega_T}{Q}\dot{V} + \omega_T^2 V = -M\omega_T^2\dot{I}_q + \frac{1}{C_T}\dot{I}_b(t) \; . \tag{15}$$

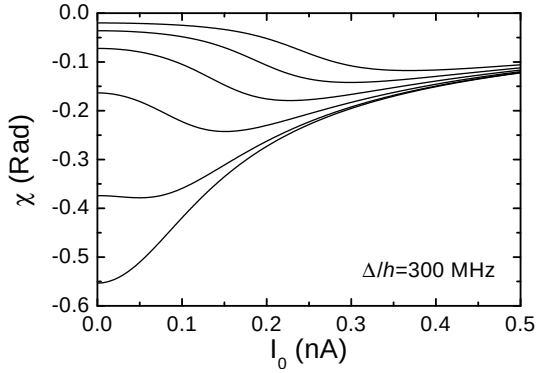

FIG. 5: Tank phase χ vs bias amplitude I_0; $\Delta/h = 300$ MHz. From the lower to the upper curve, the bias flux $10^4 f_{\rm x}$ takes the values $0, 2, 4, 6, 8, 10$.

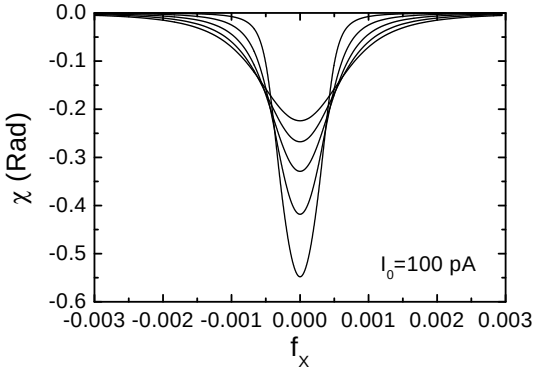

FIG. 6: Tank phase χ vs bias flux $f_{\rm x}$; $I_0 = 100$ pA. From the lower to the upper curve (at $f_{\rm x} = 0$), the tunneling frequency Δ/h takes the values $150, 300, 450, 600, 750$ MHz.

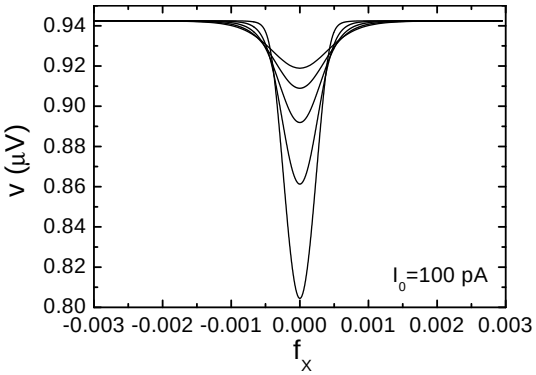

FIG. 7: Tank voltage v vs bias flux $f_{\rm x}$; $I_0 = 100$ pA. From the lower to the upper curve (at $f_{\rm x} = 0$), the tunneling frequency Δ/h takes the values $150, 300, 450, 600, 750$ MHz.

Here, $Q = \omega_{\rm T} R_{\rm T} C_{\rm T} \gg 1$ and $\omega_{\rm T} = 1/\sqrt{L_{\rm T} C_{\rm T}}$; $I_{\rm q}$ is given by (13) or (14), and depends on the qubit flux $\Phi = \Phi_{\rm x} + M I_L$, where $I_L = L_{\rm T}^{-1} \int V\, dt$ is the current in $L_{\rm T}$ and $\Phi_{\rm x}$ is time independent. Below we study the simplest case $k_{\rm B}T \ll \Delta$, so that the qubit is definitely in its ground state E_-. Then, Eq. (15) takes the form

$$\ddot{V} + \frac{\omega_{\rm T}}{Q}\dot{V} + \omega_{\rm T}^2 V = -k^2 L \omega_{\rm T}^2 \frac{d^2 E_-}{d\Phi^2} V + \frac{1}{C_{\rm T}} \dot{I}_b(t) \quad (16)$$

where $k^2 \equiv M^2/L L_{\rm T}$,

$$\frac{d^2 E_-}{d\Phi^2} = \frac{I_{\rm c}^2 \Delta^2 \lambda^2(\alpha)}{(2\pi)^2 \left(E_{\rm J}^2 f^2 \lambda^2(\alpha) + \Delta^2\right)^{3/2}} , \quad (17)$$

and $f = [\Phi_{\rm x} + M I_L(t)]/\Phi_0 - \frac{1}{2}$ ($|f| \ll 1$). Thus, (16) is nonlinear in V. Since the coupling to the qubit is small one may apply the method of harmonic balance, which is well known in rf-SQUID theory.[13] Accordingly, if $\omega \approx \omega_{\rm T}$, then V oscillates with frequency ω, while its amplitude v and phase χ are slow functions of time: $V(t) = v(t)\cos[\omega t + \chi(t)]$. From (16) we obtain

$$\dot{v} = -\frac{\omega_{\rm T} v}{2Q} + \frac{I_0 \cos\chi}{2C_{\rm T}} \quad (18)$$

$$\dot{\chi} = \omega_{\rm T}\xi_0 - \frac{I_0 \sin\chi}{2vC_{\rm T}} - \frac{k^2 \omega_{\rm T} L I_{\rm c}^2}{2\Delta} \left(\frac{\lambda(\alpha)}{2\pi}\right)^2 F(v, f_{\rm x}) \quad (19)$$

with the detuning $\xi_0 = (\omega_{\rm T} - \omega)/\omega_{\rm T}$, and where

$$F(v, f_{\rm x}) = \frac{1}{\pi} \int_0^{2\pi} d\phi\, \frac{\cos^2\phi}{\left[1 + \eta^2 \left(f_{\rm x} + \gamma \sin\phi\right)^2\right]^{3/2}} , \quad (20)$$

with $\eta = E_{\rm J}\lambda(\alpha)/\Delta$ and $\gamma = M v/\omega_{\rm T} L_{\rm T} \Phi_0$.

Setting $\dot{v} = \dot{\chi} = 0$ in (18) and (19) one obtains the stationary tank voltage and phase,

$$v^2 \left(1 + 4Q^2 \xi^2(v, f_{\rm x})\right) = I_0^2 \omega_{\rm T}^2 L_{\rm T}^2 Q^2 \quad (21)$$

$$\tan\chi = 2Q\xi(v, f_{\rm x}) , \quad (22)$$

where we introduced a flux-dependent detuning

$$\xi(v, f_{\rm x}) = \xi_0 - k^2 \frac{L I_{\rm c}^2}{2\Delta} \left(\frac{\lambda(\alpha)}{2\pi}\right)^2 F(v, f_{\rm x}) . \quad (23)$$

We have used Eqs. (21)–(23) to find voltage–flux $v(f_x)$, phase–current $\chi(I_0)$, and phase–flux $\chi(f_{\rm x})$ characteristics at resonance $\omega = \omega_{\rm T}$. We take the qubit parameters $I_{\rm c} = 400$ nA, $\alpha = 0.8$, $L = 15$ pH, $g = 100$, a tank with $L_{\rm T} = 50$ nH, $Q = 1000$, $\omega_{\rm T}/2\pi = 30$ MHz, and $k = 10^{-2}$. The $\chi(I_0)$ curves for several $f_{\rm x}$ are shown in Fig. 5. The $\chi(f_{\rm x})$ and $v(f_x)$ curves are shown in Figs. 6 and 7 for various Δ. The sharp dips in Figs. 6 and 7 correspond to the spike in the second derivative of the energy profile in Fig. 3b. Clearly, the width of the dips is correlated with Δ: with the increase of Δ the width of the dips also increases. The $\chi(f_{\rm x})$ curves for different I_0 are shown in Fig. 8. The shape and the value of χ are seen to be very sensitive to I_0. The dependence of the voltage modulation $\delta v \equiv v(f_{\rm x}{=}0) - v(f_{\rm x}{=}10^{-3})$ on I_0 is shown in Fig. 9.

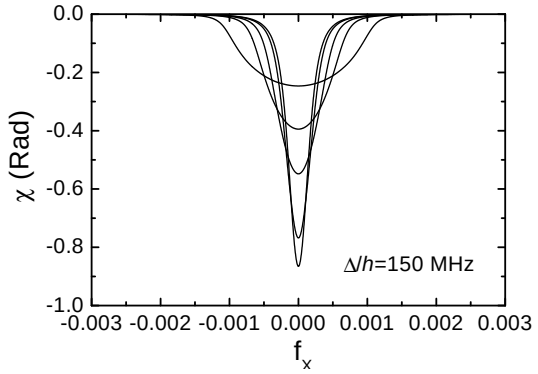

FIG. 8: Tank phase χ vs bias flux $f_{\rm x}$; $\Delta/h = 150$ MHz. From the lower to the upper curve (at $f_{\rm x} = 0$), the bias amplitude I_0 takes the values $10, 50, 100, 150, 250$ pA.

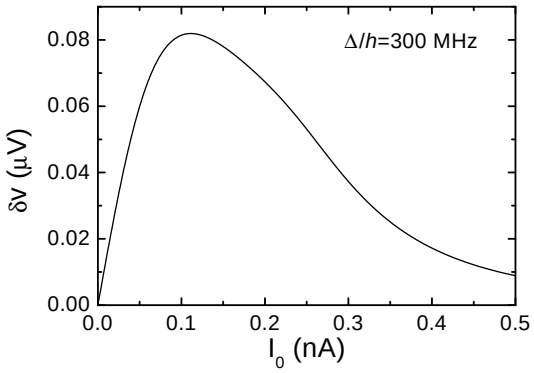

FIG. 9: Voltage modulation $\delta v = v(f_{\rm x}{=}0) - v(f_{\rm x}{=}10^{-3})$ vs bias current I_0; $\Delta/h = 300$ MHz.

B. Scheme with separate driving coil

In this scheme, a bias flux $\Phi_{\rm b}(t) = \Phi_{\rm ac} \sin \omega t$ is applied to the qubit loop from a separate coil (Fig. 10). The tank response is similar to (16):

$$\ddot{V} + \frac{\omega_{\rm T}}{Q}\dot{V} + \omega_{\rm T}^2 V = \left[-M\omega_{\rm T}^2 \frac{d^2 E_-}{d\Phi^2}\Phi_{\rm ac} + \widetilde{\Phi}_{\rm ac}\right] \omega \cos \omega t \ , \tag{24}$$

where $\widetilde{\Phi}_{\rm ac}$ is the flux which the external coil couples directly into the tank and $d^2_\Phi E_-$ is given by (17) with $f = (\Phi_{\rm x}{+}\Phi_{\rm ac} \sin \omega t)/\Phi_0 - \frac{1}{2} \equiv f_{\rm x} + f_{\rm ac} \sin \omega t$. Rewriting the first term on the rhs of (24) as

$$-k \frac{I_{\rm c}^2}{\Delta} \sqrt{L_{\rm T} L} \left(\frac{\lambda}{2\pi}\right)^2 \omega_{\rm T}^2 \omega \Phi_0 f_{\rm ac} G(t) \tag{25}$$

makes its time dependence manifest:

$$G(t) = \frac{\cos \omega t}{\left[1 + \eta^2 \left(f_{\rm x} + f_{\rm ac} \sin \omega t\right)^2\right]^{3/2}} \ . \tag{26}$$

The advantage of a separate driving coil is that one can effectively decouple the tank from the fundamental harmonic of the bias, since the qubit signal $G(t)$ contains not only ω but also 2ω, 3ω, etc. At $f_{\rm x} = 0$, $G(t)$ contains only odd harmonics. This can be used to find the degeneracy point in practice, e.g., by tuning $f_{\rm x}$ so that the tank response vanishes (reaches its maximum) at frequency 2ω (3ω). We have studied the higher harmonics by solving Eq. (24) numerically with $\widetilde{\Phi}_{\rm ac} = 0$ for $\omega = \omega_{\rm T}/2$ and $\omega = \omega_{\rm T}/3$, see Fig. 11. Since the full amplitudes contain contributions from all harmonics, at $\omega = \omega_{\rm T}/2$, $f_{\rm x} = 0$ one observes a finite dip rather than a zero.

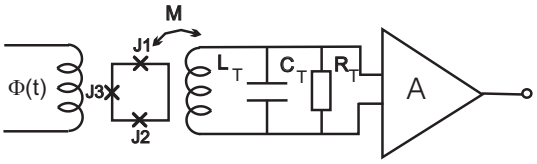

FIG. 10: Flux qubit coupled to a tank: scheme with a separate driving coil.

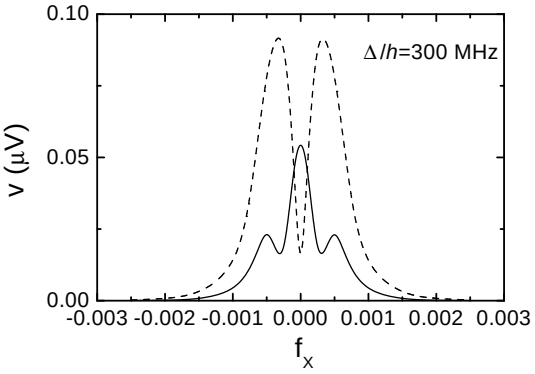

FIG. 11: Tank voltage vs bias flux $f_{\rm x}$; $\Delta/h = 300$ MHz, $\Phi_{\rm ac} = 5 \cdot 10^{-4}\Phi_0$. Dotted line: driving frequency $\omega = \omega_{\rm T}/2$; solid line: $\omega = \omega_{\rm T}/3$.

IV. REQUIREMENTS ON NOISE SOURCES

Figures 6 and 7 clearly reveal the quantum nature of the flux qubit within a range $|\delta f_{\rm x}| \leq 5 \cdot 10^{-4}$ from the degeneracy point $f_{\rm x} = 0$. Therefore, the unavoidable external flux noise coupled to the qubit must be much smaller than this value. The most important sources are the Nyquist noise $I_{\rm n} = \sqrt{4k_{\rm B}T/R_{\rm T}}$ and the current noise $I_{\rm a}$ of the preamplifier. The former generates the qubit-flux noise $\Phi_{\rm n} = MI_{\rm n}Q\sqrt{B}$, where $B = \omega_{\rm T}/2\pi Q$ is the tank bandwidth. With $T = 20$ mK and the tank parameters of Section III, one gets $\Phi_{\rm n} \approx 8 \cdot 10^{-6}\Phi_0$. For $I_{\rm a} = 10^{-14}{\rm A}/\sqrt{\rm Hz}$, we estimate the corresponding flux noise as $\Phi_{\rm a} = MI_{\rm a}Q\sqrt{B} \approx 7 \cdot 10^{-6}\Phi_0$. Thus, the noise these sources couple to the qubit is at least two orders smaller than the peak widths in Figs. 6 and 7. On the other hand, these sources give rise to directly detected voltage noise across the tank circuit. The thermal tank noise is $V_{\rm n} = I_{\rm n}\omega_{\rm T}L_{\rm T}Q\sqrt{B} \approx 17.6$ nV. The noise due to $I_{\rm a}$ is $V_{\rm a1} = I_{\rm a}\omega_{\rm T}L_TQ\sqrt{B} \approx 16$ nV. And finally, if we

take $V_{a2} = 40\ \mathrm{pV}/\sqrt{\mathrm{Hz}}$ for the preamplifier's own voltage noise, we get $V_{a2}\sqrt{B} \approx 7$ nV for its contribution in the tank bandwidth. Comparing these values with the voltage modulation in Figs. 7, 9, and 11, we see they are at least several times smaller than the qubit signal.

V. CONCLUSION

We have shown that IMT can be used for low-frequency characterization of the ground (in general: equilibrium) state of a flux qubit. The method allows determining the tunnel splitting between qubit states for a broad class of devices; with the term "flux (as opposed to phase) qubit" we stress that the two states must differ not only in Josephson phase, but in actual magnetic flux visible to the outside.[1] The design exclusively employs present-day technology, and the expected noise levels have been shown not to disrupt the measurement. On the qubit time scale, the method is a quasi-equilibrium one; as such, it can determine Δ but not, e.g., the "T_2" dephasing time.[14] Efforts to adapt IMT to this and related problems such as qubit readout and control are underway.

Acknowledgments

We thank A.Yu. Smirnov and A.M. Zagoskin for detailed discussions.

* On leave from Novosibirsk State Technical University, 20 K. Marx Ave., 630092 Novosibirsk, Russia.
† On leave from Department of Solid State Physics, Comenius University, SK-84248 Bratislava, Slovakia.
‡ Electronic address: ilichev@ipht-jena.de

[1] Yu. Makhlin, G. Schön, and A. Shnirman, Rev. Mod. Phys. **73**, 357 (2001).
[2] G. Blatter, V.B. Geshkenbein, and L.B. Ioffe, Phys. Rev. B **63**, 174511 (2001).
[3] M.J. Feldman and M.F. Bocko, Physica C **350**, 171 (2001); J.R. Friedman, V. Patel, W. Chen, S.K. Tolpygo, and J.E. Lukens, Nature **406**, 43 (2000); M.V. Fistul, submitted to Physica Status Solidi.
[4] T.P. Orlando, J.E. Mooij, L. Tian, C.H. van der Wal, L. Levitov, S. Lloyd, and J.J. Mazo, Phys. Rev. B **60**, 15398 (1999).
[5] C.H. van der Wal, A.C.J. ter Haar, F.K. Wilhelm, R.N. Schouten, C.J.P.M. Harmans, T.P. Orlando, S. Lloyd, and J.E. Mooij, Science **290**, 773 (2000).
[6] M.H.S. Amin, A.N. Omelyanchouk, A. Blais, A. Maassen van den Brink, G. Rose, T. Duty, and A.M. Zagoskin, Physica C **368**, 310 (2002).
[7] H. Tanaka, Y. Sekine, S. Saito, and H. Takayanagi, Physica C **368**, 300 (2002).
[8] E. Il'ichev, Th. Wagner, L. Fritzsch, J. Kunert, V. Schultze, T. May, H.E. Hoenig, H.-G. Meyer, M. Grajcar, D. Born, W. Krech, M.V. Fistul, and A.M. Zagoskin, Appl. Phys. Lett. **80**, 4184 (2002).
[9] R. Rifkin and B.S. Deaver, Phys. Rev. B **13**, 3894 (1976).
[10] E. Il'ichev, V. Zakosarenko, L. Fritzsch, R. Stolz, H.E. Hoenig, H.-G. Meyer, M. Gotz, A.B. Zorin, V.V. Hanin, A.B. Pavolotsky, and J. Niemeyer, Rev. Sci. Instr. **72**, 1882 (2001).
[11] E.g., T.D. Clark, J. Diggins, J.F. Ralph, M. Everitt, R.J. Prance, H. Prance, R. Whiteman, A. Widom, and Y.N. Srivastava, Ann. Phys. **268**, 1 (1998).
[12] J.E. Mooij, T.P. Orlando, L. Levitov, L. Tian, C.H. van der Wal, and S. Lloyd, Science **285**, 1036 (1999).
[13] K.K. Likharev, *Dynamics of Josephson Junctions and Circuits* (Gordon and Breach, New York, 1986).
[14] A. Maassen van den Brink, in preparation.